



How the O₂-dependent Mg-protoporphyrin monomethyl ester cyclase forms the fifth ring of chlorophylls

Guangyu E. Chen^{1,3}✉, Nathan B. P. Adams¹, Philip J. Jackson^{1,2}, Mark J. Dickman² and C. Neil Hunter¹✉

Mg-protoporphyrin IX monomethyl ester (MgPME) cyclase catalyses the formation of the isocyclic ring, producing protochlorophyllide_a and contributing substantially to the absorption properties of chlorophylls and bacteriochlorophylls. The O₂-dependent cyclase is found in both oxygenic phototrophs and some purple bacteria. We overproduced the simplest form of the cyclase, AcsF, from *Rubrivivax gelatinosus*, in *Escherichia coli*. In biochemical assays the di-iron cluster within AcsF is reduced by ferredoxin furnished by NADPH and ferredoxin:NADP⁺ reductase, or by direct coupling to Photosystem I photochemistry, linking cyclase to the photosynthetic electron transport chain. Kinetic analyses yielded a turnover number of 0.9 min⁻¹, a Michaelis-Menten constant of 7.0 μM for MgPME and a dissociation constant for MgPME of 0.16 μM. Mass spectrometry identified 13¹-hydroxy-MgPME and 13¹-keto-MgPME as cyclase reaction intermediates, revealing the steps that form the isocyclic ring and completing the work originated by Sam Granick in 1950.

Chlorophylls, a class of cyclic tetrapyrroles, are among the most abundant natural pigments on Earth. They are the major absorbers of the solar energy that drives photosynthesis, and billions of tonnes of chlorophyll are synthesized annually on land and in the oceans. The decisive biosynthetic step that determines the absorptive properties of chlorophyll, and more visually its green colour, is the formation of the unique isocyclic fifth ring. This process involves the conversion of Mg-protoporphyrin IX monomethyl ester (MgPME) to 3,8-divinyl protochlorophyllide_a (DV PChlide_a), and requires incorporation of an oxygen atom sourced from either water or O₂ (refs. ^{1,2}), indicating the existence of two mechanistically different MgPME cyclases. Most anoxygenic phototrophic bacteria utilize an O₂-sensitive radical SAM enzyme containing [4Fe-4S] and cobalamin co-factors to catalyse the reaction³, while oxygenic phototrophs including cyanobacteria, algae and plants, as well as some purple bacteria, adopt an O₂-dependent cyclase for the reaction. Three classes of O₂-dependent cyclase have been identified⁴, all with a catalytic subunit AcsF, a putative di-iron protein⁵, but they differ in the requirement for an auxiliary subunit, either Ycf54 for the enzyme found in oxygenic phototrophs^{6,7} or BciE for the alphaproteobacterial enzyme⁴. However, because there have been no mechanistic studies of the O₂-dependent cyclase using purified components, details of this important reaction have remained unknown since Granick⁸ proposed a sequence of reactions that form the isocyclic fifth, or E, ring.

Early biochemical characterization of cyclase activity using either intact or fractionated chloroplasts demonstrated the necessity for O₂ (refs. ^{9–12}), and inhibitor studies with specific chelators showed that iron is also required¹¹. Both NADPH and NADH were found to stimulate cyclase activity, with the former more effective than the latter^{11,13}. These properties are shared by enzymes from the green alga *Chlamydomonas* (*C.*) *reinhardtii* and the cyanobacterium

Synechocystis sp. PCC 6803 (hereafter *Synechocystis*)^{14,15}, and are characteristic of iron-dependent oxygenases. In addition, although cucumber, *Synechocystis* and barley enzymes were resolved into soluble and membrane-bound components^{13,15,16}, it has not been possible to obtain an active, pure cyclase from a native source.

The complexity of E ring formation implies the involvement of multiple sequential reactions. Based on the mechanism of β-oxidation of fatty acids, Granick⁸ proposed that the reaction could proceed through β-oxidation of the C13 methylpropionyl group of MgPME via the intermediates 13¹–13² acrylate, 13¹-hydroxy and 13¹-keto. These proposed reaction intermediates were subsequently detected in certain *Chlorella* mutants^{17,18}, and Castelfranco and co-workers confirmed the 13¹-hydroxy and 13¹-keto intermediates using the reconstituted cucumber cyclase system¹⁹. The 13¹-hydroxy derivative of MgPME was detected in these assays and was shown to be an active cyclase substrate, and a similar compound was also identified during measurements of cyclase activity in isolated chloroplasts from *C. reinhardtii*¹⁴. A chemically synthesized 13¹-keto analogue of MgPME is readily converted to the final cyclase product, thereby validating this intermediate in the reaction sequence¹⁹. However, a synthesized acrylate derivative of MgPME was found to be inactive as a cyclase substrate in the reconstituted cyclase system²⁰. It is possible that the acrylate derivative detected in the *Chlorella* mutants resulted from the 13¹-hydroxy intermediate undergoing a reverse hydratase reaction¹. Based on these findings, the original reaction scheme of Granick and others has been modified to omit the acrylate intermediate, as shown in Fig. 1.

Elucidation of the cyclase reaction sequence requires quantities of pure, active enzyme sufficient for biochemical and kinetic analyses. Although there have been no reports of the purification and in vitro reconstitution of the O₂-dependent cyclase, an active recombinant cyclase was used successfully as part of a complete

¹Department of Molecular Biology and Biotechnology, University of Sheffield, Sheffield, UK. ²Department of Chemical and Biological Engineering, University of Sheffield, Sheffield, UK. ³Present address: School of Life Sciences and Biotechnology, Shanghai Jiao Tong University, Shanghai, China. ✉e-mail: guangyu.chen@sju.edu.cn; c.n.hunter@sheffield.ac.uk

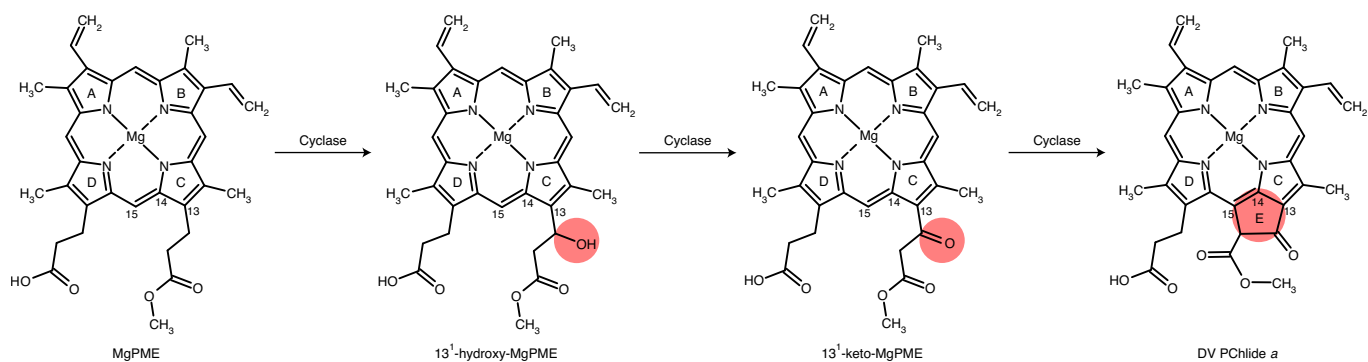


Fig. 1 | Proposed reaction intermediates of MgPME cyclase. Formation of the E ring of chlorophyll is proposed to proceed via hydroxylation, oxidation and cyclization of the C13 methylpropionyl side chain of MgPME. The chemical change at each step is highlighted. International Union of Pure and Applied Chemistry numbering of the relevant macrocycle carbons is indicated.

ensemble of biosynthetic enzymes that collectively enabled the synthesis of chlorophyll by *E. coli*²¹. Here we report the purification of the single-subunit, O₂-dependent cyclase AcsF from *Rubrivivax (Rvi.) gelatinosus*⁵. Cyclase activity was reconstituted using a tri-component electron transfer system consisting of NADPH, ferredoxin (Fd) and Fd:NADP⁺ reductase (FNR), and the steady-state kinetic behaviour of the enzyme was characterized. Furthermore, we detected the two previously proposed reaction intermediates in the progress of the reaction and subsequently determined their chemical identity by mass spectrometry. Our work therefore lays the groundwork for future mechanistic and structural studies of the O₂-dependent cyclase involved in chlorophyll biosynthesis.

Purification of AcsF from *Rvi. gelatinosus*

Rubrivivax gelatinosus AcsF with an N-terminal His₆ tag was produced in the *E. coli* strain C43(DE3)²², supplemented with ferric ammonium citrate (Methods). His-tagged AcsF was purified by Ni-iminodiacetic acid affinity chromatography from membrane fractions solubilized with the non-ionic detergent *n*-dodecyl- β -D-maltoside (β -DDM), followed by an iron reconstitution step with ferrous ammonium sulphate to increase occupancy of the iron-binding sites. Subsequent gel filtration chromatography, in which a single symmetrical elution peak was observed (Fig. 2a), purified AcsF further. SDS-polyacrylamide gel electrophoresis (PAGE) analysis showed a single polypeptide with an apparent molecular mass of ~37 kDa (Fig. 2a, inset), and migration further through the gel than expected for a predicted mass of 44 kDa, a common feature of membrane-associated proteins. The protein was >95% pure, with an overall yield of ~3 mg l⁻¹ culture.

To investigate the oligomerization state of the purified AcsF protein, gel filtration calibration curves were produced by analysis of commercially available soluble protein standards and four membrane protein standards available in our laboratory (Fig. 2b). We assumed that the collective mass of β -DDM molecules in complex with membrane proteins is the same as a β -DDM micelle, which is 72 ± 1.4 kDa (ref. 23). The purified AcsF with the associated β -DDM molecules was estimated to have a molecular mass of ~210 kDa with soluble standards, and ~180 kDa using membrane protein standards (Fig. 2b). By subtracting the contribution from detergent molecules, this indicates that AcsF is dimeric or trimeric given the predicted molecular mass of 44 kDa from the primary sequence.

Spectroscopic and biophysical characterization of AcsF

Purified AcsF has a pale brown colour and exhibits a broad and weak band centred at ~340 nm in the absorbance spectrum (Fig. 2c), which is from an oxo-to-Fe(III) charge transfer transition²⁴. An additional band at ~410 nm was also observed (Fig. 2c). Following

the addition of 2 M sodium azide, the formation of a chromophore with broad absorbance bands at 345 and 450 nm was observed while the position of the ~410-nm band was unaffected (Fig. 2d). The optical features, including the ~340-nm charge transfer band and the 345- and 450-nm bands when in complex with azide, are characteristic of μ -oxo-bridged di-iron clusters that have been reported for other di-iron proteins such as stearyl-acyl carrier protein Δ^9 desaturase²⁴, CmlA in chloramphenicol biosynthesis²⁵ and CLK-1 in ubiquinone biosynthesis²⁶. Assays determined that AcsF contained 2.35 ± 0.04 iron atoms per monomer (Supplementary Fig. 1), providing further evidence for the presence of a di-iron cluster in AcsF. We used differential scanning calorimetry to analyse the thermostability of AcsF and the melting point was determined to be 57.2 °C (Supplementary Fig. 2), indicating that the protein is stable for activity tests at 30 °C.

In vitro reconstitution of cyclase activity with AcsF

To test whether purified AcsF is active, we conducted end-point in vitro assays followed by pigment analysis using high-performance liquid chromatography (HPLC). Apart from the porphyrin substrate, MgPME and molecular oxygen, an electron donor is also required to reduce the di-iron centre of AcsF from +3 to +2 during the catalytic cycle as required by most other di-iron enzymes. An NADPH electron donor was suggested by early cyclase assays using biochemical fractions from *Synechocystis*, *C. reinhardtii* and plants^{13,15}, but no activity was detected using only AcsF and NADPH (Fig. 2e, fourth trace from top), suggesting that it is not directly involved in cyclase activity. Guided by the findings that several di-iron enzymes accept electrons from reduced Fd for activity^{27,28}, we combined spinach Fd and FNR with NADPH to form a tri-component Fd reduction system, which did support the cyclase activity of AcsF (Fig. 2e, top trace). The activity is dependent on the presence of NADPH, Fd, FNR and AcsF, as indicated by the control assays (Fig. 2e, second, third, fourth and fifth traces from the top, respectively). Next, we scaled up the assay and increased the MgPME concentration from 10 to 27 μ M. The catalytic activity of AcsF was clearly demonstrated by the dramatic colour change of the assay mixture, indicating a probable complete conversion with only a 30-min incubation (Fig. 2f).

Steady-state kinetic behaviour and porphyrin binding of AcsF

The dramatic colour change from red to green following product formation allowed us to develop an absorption-based continuous assay to investigate the steady-state kinetic behaviour of AcsF. We switched to a cyanobacterial source of Fd and FNR by overexpressing the genes from *Anabaena* sp. PCC 7119 (hereafter *Anabaena*) in

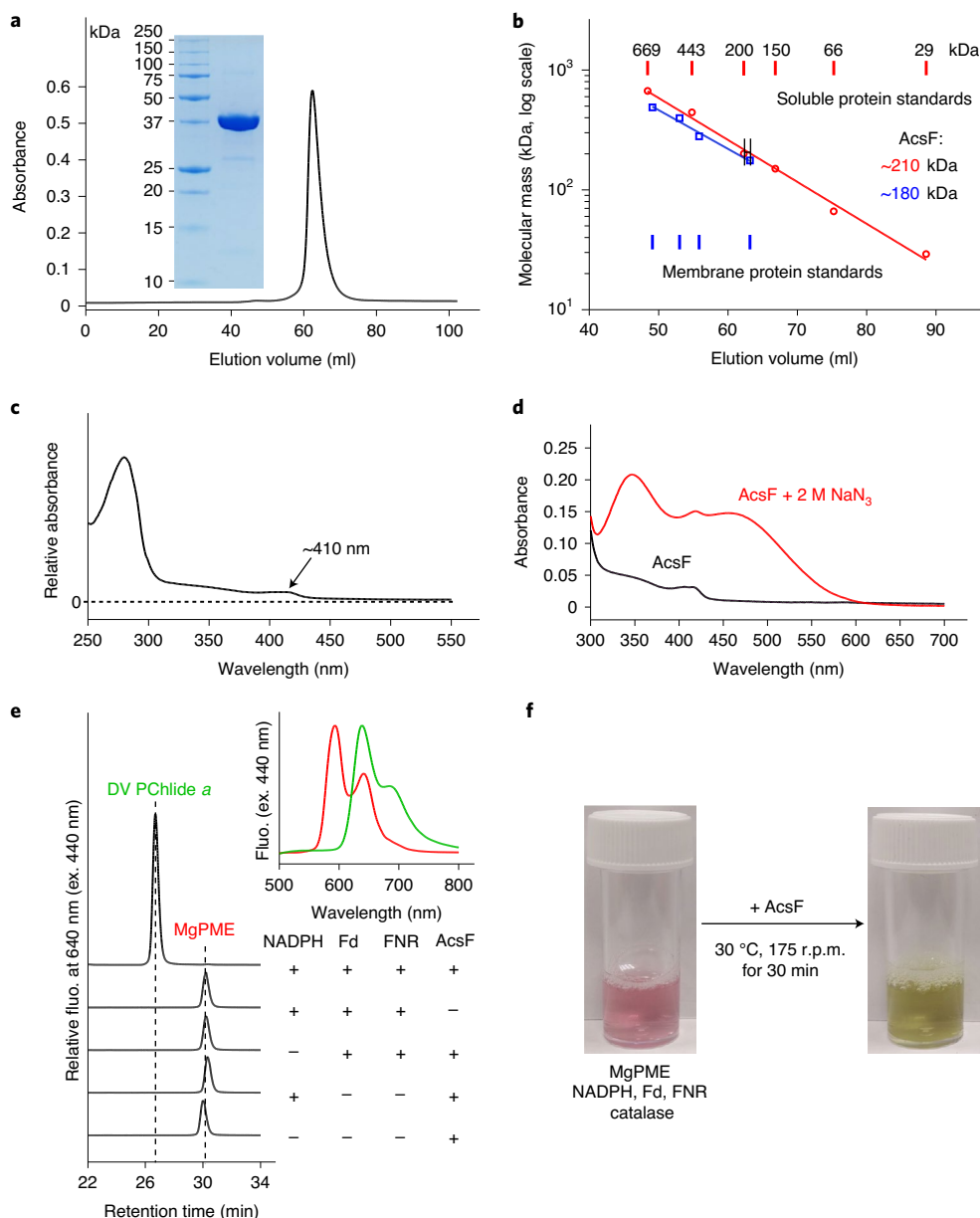


Fig. 2 | Purification, spectral characterization and reconstitution of AcsF cyclase activity. **a**, Gel filtration profile of AcsF on a HiLoad 16/600 Superdex 200 prep-grade column, monitored by absorbance at 280 nm and SDS-PAGE analysis of 10 μg of purified AcsF (inset). Shown are representative of three independently repeated experiments. **b**, Estimate of the molecular mass of native AcsF from triplicate gel filtration runs (range of elution volume indicated) using calibration curves (logarithm of molecular mass versus elution volume) generated from the data points of soluble (red circles) and membrane (blue squares) protein standards using nonlinear regression analysis. Membrane protein standards of 104, 208, 325 and 416 kDa were used, and a value of 72 kDa (size of β -DDM micelles) was added to each molecular mass when generating the calibration curve. The calculated molecular mass values (inset) include the contribution of bound β -DDM molecules. **c**, Absorbance spectrum of AcsF as isolated. **d**, Absorbance spectra of 8 μM AcsF in the absence and presence of 2 M sodium azide. **e**, Co-factor requirements for in vitro cyclase activity of AcsF revealed by end-point HPLC-based assays. A complete assay contained 3.7 μM AcsF, 10 μM MgPME, 2 mM NADPH, 0.2 mg ml^{-1} spinach Fd, 0.4 U ml^{-1} spinach FNR and 0.29 mg ml^{-1} catalase. Retention times and fluorescence (flu.) spectra (inset) with excitation (ex.) at 440 nm were used to identify pigment species. Experimental details are provided in Methods. **f**, Photographs showing marked colour change indicating the activity of AcsF in an assay containing 27 μM MgPME and other assay components at the same concentrations as in **a**.

E. coli (Extended Data Fig. 1 shows the electrophoretic analysis and absorbance spectra of purified *Anabaena* Fd and FNR). Test assays monitored the spectral changes and found a clear trend of decreased absorbance maxima of the substrate at 422, 552 and 592 nm, accompanied by increased absorbance maxima for the product at 446, 586 and 634 nm (Fig. 3a). The initial rate of product formation was calculated by quantification of DV PChlide *a* absorbance at 634 nm using

a reported extinction coefficient^{29,30}. We observed clear linear dependency of the initial rate with respect to AcsF concentration (Fig. 3b). As the electron mediator between NADPH and AcsF, Fd was found to be rate limiting. The initial rate displayed a hyperbolic response to Fd, with an apparent K_M determined to be $4.05 \pm 0.39 \mu\text{M}$ in the presence of 0.17 μM FNR, or $2.41 \pm 0.26 \mu\text{M}$ with 1.7 μM FNR (Fig. 3c). In subsequent assays, Fd was used at a saturating concentration of

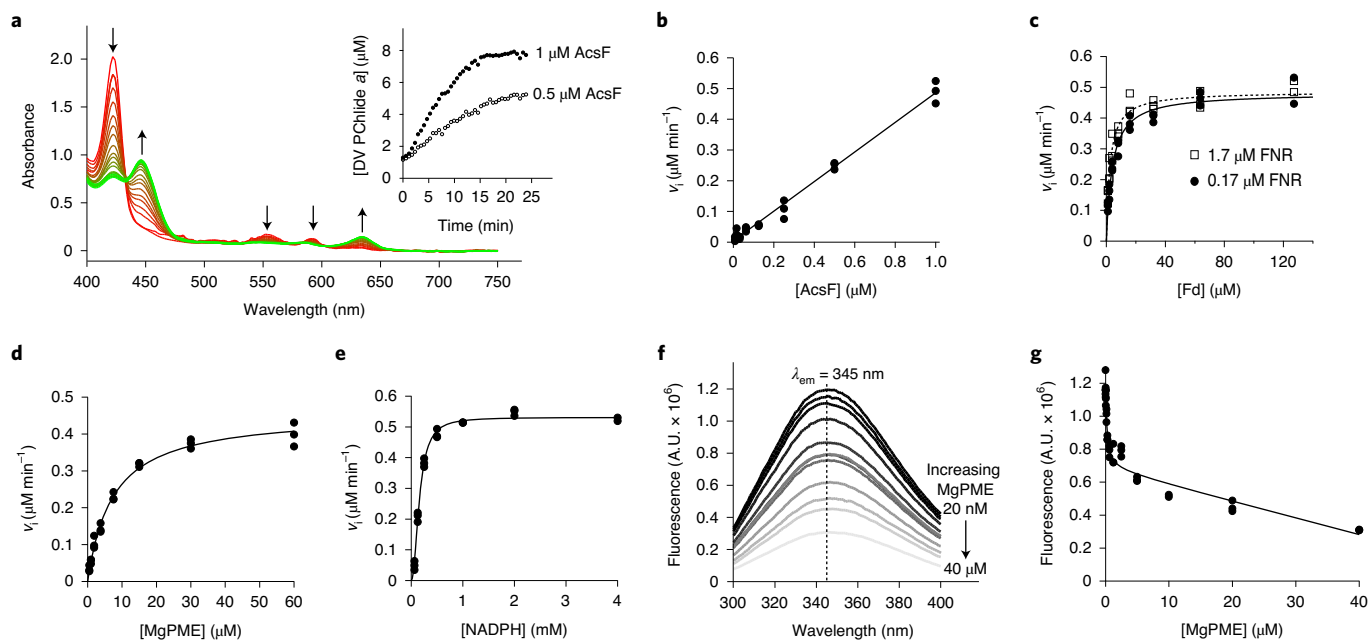


Fig. 3 | Steady-state kinetics of AcsF, and binding of MgPME to AcsF analysed by tryptophan fluorescence quenching. **a**, Progressive spectral change during a continuous, absorbance-based cyclase assay containing 1 μM AcsF, 10 μM MgPME, 7.6 μM *Anabaena* Fd, 0.17 μM *Anabaena* FNR, 2.5 mM NADPH and 0.29 mg ml^{-1} catalase. Arrows indicate the direction of change. Inset shows the evolution of product (DV PChlide *a*) with 0.5 and 1 μM AcsF, monitored by absorbance at 634 nm. **b–e**, Dependence of the initial rate of product formation on AcsF (**b**), *Anabaena* Fd (**c**), MgPME (**d**) and NADPH (**e**). Assay conditions were as in **a** except for the following differences: **b**, 7.81 nM–1 μM AcsF; **c**, 0.5 μM AcsF, 0.17 or 1.7 μM *Anabaena* FNR and 0.99–127 μM *Anabaena* Fd; **d**, 0.5 μM AcsF, 1.7 μM *Anabaena* FNR and 31 μM *Anabaena* Fd; **e**, 0.5 μM AcsF, 30 μM MgPME, 1.7 μM *Anabaena* FNR, 31 μM *Anabaena* Fd and 62.5 μM –4 mM NADPH. Each data point is an independent experiment. **c, d**, The Michaelis–Menten equation (equation (1); Methods) was fitted to the kinetic data with the characterizing parameters K_M (apparent) = $4.05 \pm 0.39 \mu\text{M}$ (0.17 μM FNR) or $2.41 \pm 0.26 \mu\text{M}$ (1.7 μM FNR) (**c**); $k_{\text{cat}}^{\text{MgPME}} = 0.91 \pm 0.02 \text{ min}^{-1}$ and $K_M^{\text{MgPME}} = 7.03 \pm 0.51 \mu\text{M}$ (**d**). The Hill equation (equation (2); Methods) was fitted to the NADPH titration data with $k_{\text{cat}}^{\text{NADPH}} = 1.06 \pm 0.01 \text{ min}^{-1}$ and $K_{0.5}^{\text{NADPH}} = 0.16 \pm 0.01 \text{ mM}$, $n = 2.1 \pm 0.1$ (**e**). **f**, A series of spectra showing quenching of AcsF fluorescence by MgPME. Excitation was set at 280 nm, producing an emission maximum (λ_{em}) at 345 nm. The average fluorescence spectra of triplicate experiments are shown. **g**, Plot of AcsF fluorescence against MgPME concentration. Each data point is an independent experiment. The curve fit is described by a modified single-site binding model (equation (3); Methods) with K_d for MgPME binding of $0.16 \pm 0.05 \mu\text{M}$. A.U., arbitrary units.

31 μM along with 1.7 μM FNR. The dependence of the initial rate on MgPME followed Michaelis–Menten kinetics, with these characterizing parameters: turnover number (k_{cat}) = $0.91 \pm 0.02 \text{ min}^{-1}$, Michaelis–Menten constant (K_M) = $7.03 \pm 0.51 \mu\text{M}$ and $k_{\text{cat}}/K_M = 0.13 \pm 0.01 \mu\text{M}^{-1} \text{ min}^{-1}$ (Fig. 3d). Since a sigmoidal relationship was found between the initial rate and NADPH concentration, the Hill equation was used to fit the kinetic data with $k_{\text{cat}} = 1.06 \pm 0.01 \text{ min}^{-1}$, $K_{0.5} = 0.16 \pm 0.01 \text{ mM}$, $k_{\text{cat}}/K_{0.5} = 6.64 \pm 0.21 \text{ mM}^{-1} \text{ min}^{-1}$ and the Hill coefficient $n = 2.1 \pm 0.1$ (Fig. 3e).

Because AcsF is the only subunit of the cyclase, we quantified the binding affinity for the porphyrin substrate, MgPME, by measuring tryptophan fluorescence quenching of AcsF following binding of MgPME. With increasing concentrations of MgPME, the degree of quenching gradually intensified (Fig. 3f). The titration data fit a single-site binding model with modifications to include the inner filter effect of MgPME^{31,32}, giving a K_d of $0.16 \pm 0.05 \mu\text{M}$ for MgPME binding (Fig. 3g).

Identification of the reaction intermediates of AcsF

Apart from MgPME substrate and DV PChlide *a* product, some end-point cyclase assays contained two pigment species, provisionally named X1 and X2, for the ~21- and ~28-min HPLC peaks, respectively. Intriguingly, X1 had the same absorbance and fluorescence spectra as MgPME whereas the spectral characteristics of X2 were between those of MgPME and DV PChlide *a* (Fig. 4, insets). The MgPME used was highly pure and the other assay components were defined, which was supported by the absence of X1 and X2 in

the control assay without AcsF (Fig. 4). Assays with twofold escalating concentrations of AcsF were terminated after 30 min of incubation. As shown in Fig. 4, peaks X1 and X2 became apparent with increasing concentrations of AcsF, reached a maximum level then gradually disappeared, while the DV PChlide *a* product continuously accumulated. The dynamics of X1 and X2 during the progress of the reaction are consistent with their potential roles as reaction intermediates. Based on their spectral features, we suspected X1 to be the hydroxy and X2 the keto reaction intermediates, as previously proposed^{8,20}.

To confirm the identity of X1 and X2, the assay with 0.92 μM AcsF (4 \times AcsF), which accumulated the two pigment species the most (Fig. 4), was scaled up and the resulting pigment extract analysed by liquid chromatography–electrospray ionization–tandem mass spectrometry (LC–ESI–MS/MS). Extracted ion chromatograms show that MgPME and DV PChlide *a*, and the putative intermediates 13¹-hydroxy-MgPME and 13¹-keto-MgPME, were baseline resolved by reverse-phase LC (Fig. 5a–d, left). Consistent with identification of the extracted ion peak at 614.2 m/z as 13¹-hydroxy-MgPME (Fig. 5b, left), its retention time at 24 min was notably earlier than the other three tetrapyrroles, as expected by the greater hydrophilicity conferred by the presence of a hydroxyl group. The non-hydroxylated tetrapyrroles were all clustered in the later, 29–33-min eluting region. Mass spectral criteria for validation of our identification of MgPME, 13¹-hydroxy-MgPME, 13¹-keto-MgPME and DV PChlide *a* are shown by comparison of the experimental and theoretical isotopomer m/z values and relative

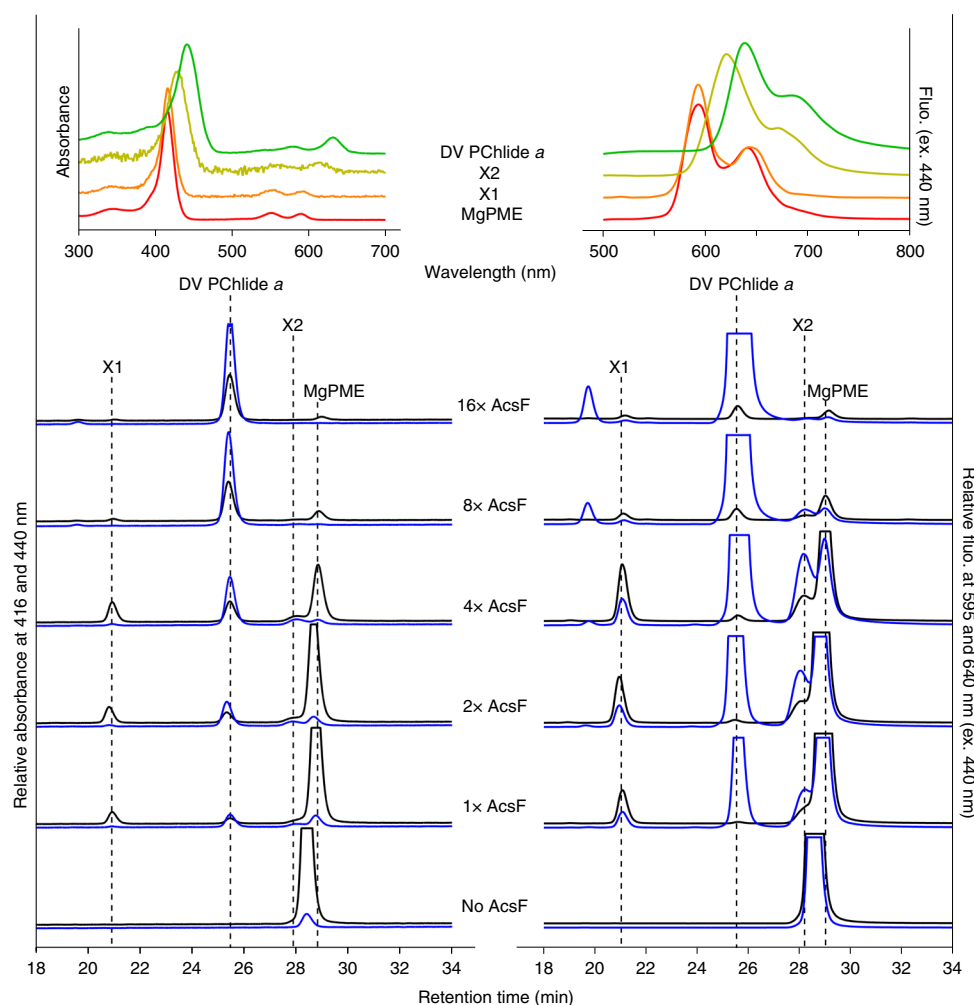


Fig. 4 | HPLC elution profiles of pigment extracts from end-point cyclase assays at various AcsF concentrations. Assay conditions were $20\ \mu\text{M}$ MgPME, $0.2\ \text{mg}\ \text{ml}^{-1}$ spinach Fd, $0.4\ \text{U}\ \text{ml}^{-1}$ spinach FNR, $2\ \text{mM}$ NADPH, $0.29\ \text{mg}\ \text{ml}^{-1}$ catalase and AcsF, at various concentrations from 0.23 (1x AcsF) to 3.68 ($16\times$ AcsF) μM . Assays were initiated by the addition of AcsF and terminated after 30 min of incubation. Pigment extracts from the assays were analysed by HPLC, with elution of pigment species monitored by absorbance at 416 (black) and 440 nm (blue) and by fluorescence (flu.) at 595 (black) and 640 nm (blue), with excitation (ex.) at 440 nm. Insets show the acquired absorbance and fluorescence spectra of MgPME, DV PChlide *a* and the potential reaction intermediates, X1 and X2.

intensities in the full MS spectra (Supplementary Fig. 3a–d, top left). The mono-isotopic ions showed accuracies of 0.49–0.84 ppm, and in three cases there was close agreement in isotopomer patterns. In the case of 13^1 -keto-MgPME (Supplementary Fig. 3c, top left), isotopomer pattern fidelity could not be assessed because the ^{13}C , and $^{13}\text{C}_2$ ions were merged with coincident unidentified ions. MgPME, 13^1 -hydroxy-MgPME and 13^1 -keto-MgPME (Supplementary Fig. 3a–c, top left) all ionized in the electrospray source to form radical cations. In the case of DV PChlide *a*, the number of neutral molecules available for radical cation formation was lowered by a dominant population of protonated cations (Supplementary Fig. 3d, top left), presumably as a result of a change in electrochemical properties following cyclization³³. Product ion spectra generated by the higher-energy C-trap dissociation (HCD) of the precursor ions indicate relatively simple neutral loss pathways for MgPME and DV PChlide *a* (Fig. 5a,d, centre and right) forming the predicted carbocation products, in which the positive charge resides on the larger fragment. No side-chain signature product ions at 59 and 73 m/z were detected. Similarly, the putative 13^1 -hydroxy-MgPME and 13^1 -keto-MgPME molecular ions dissociated without generating low- m/z signature ions, but they did form a greater number (six to

seven) of high- m/z cation products (Fig. 5b,c, centre). The increased number of potential neutral loss pathways for 13^1 -hydroxy-MgPME and 13^1 -keto-MgPME is an expected consequence of the additional functional group on the C13 methylpropionyl side chain. We further validated these two intermediates (Fig. 5b,c, right) by mapping their product ion spectra to structures generated by these neutral loss pathways (Supplementary Fig. 3b,c, bottom).

Coupling cyclase to reduced Fd produced by Photosystem I

We have shown that cyclase activity requires electrons supplied by reduced Fd (Fig. 2e) which, in oxygenic phototrophs, is generated by Photosystem I (PSI) using light energy and electrons from plastocyanin (Pc). To test for a direct link between the activities of cyclase and PSI, we conducted *in vitro* assays that couple the cyclase assay to a reconstituted PSI electron transport system³⁴ containing sodium L-ascorbate (Asc) as the reductant, 2,6-dichlorophenolindophenol (DCPIP) as the electron mediator, spinach Fd, Pc and PSI. It is intriguing that even in the absence of PSI the two cyclase reaction intermediates, 13^1 -hydroxy-MgPME and 13^1 -keto-MgPME, were detected (Extended Data Fig. 2 and Supplementary Fig. 4a). Systematic control assays showed that Asc alone was able to

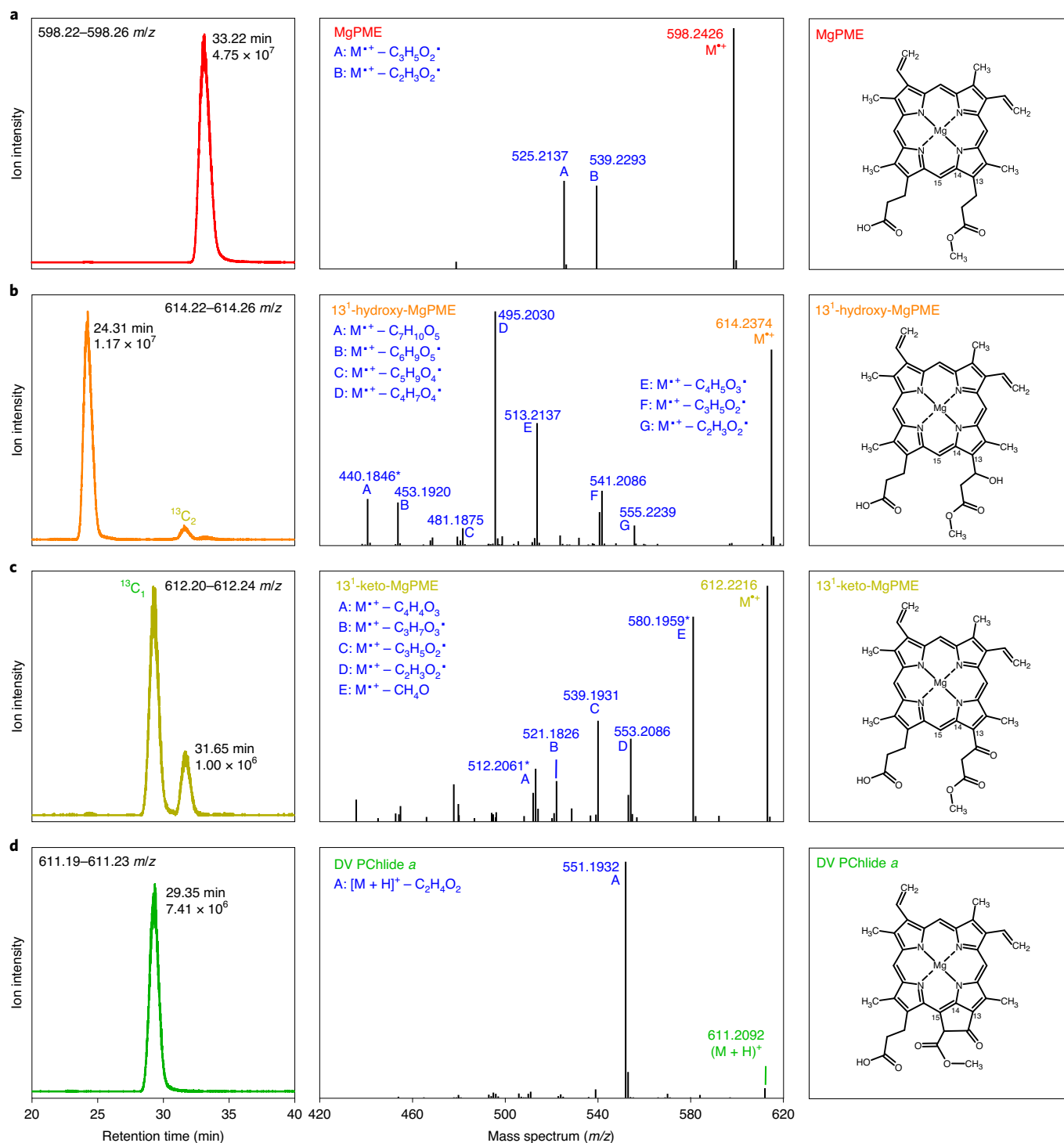


Fig. 5 | Analysis of extracted pigments by LC-ESI-MS/MS. a–d, The pigment extract from scaled-up *in vitro* cyclase assays corresponding to 4× AcSF (0.92 μ M) in Fig. 4 was analysed. Extracted ion chromatograms (EICs) and product ion spectra derived from HCD of selected mono-isotopic molecular ions are shown in the left and centre panels, respectively: MgPME (**a**), $^{13}\text{C}_1$ -hydroxy-MgPME (**b**), $^{13}\text{C}_1$ -keto-MgPME (**c**) and DV PChlide *a* (**d**). The molecular structures that align with the mass spectral evidence presented here are shown in the corresponding right-hand panels. EICs were generated for the indicated m/z ranges covering the target mono-isotopic ions, with peaks labelled by their retention times and ion intensities. Peaks mapping to ^{13}C -containing isotopomers falling within the EIC range are also labelled. Cations generated by gas phase neutral loss reactions are indicated by upper case letters, with the eliminated molecular formulae also listed. The majority of product ions are carbocations formed after radical neutral loss; those labelled with an asterisk are radical cations formed by the neutral loss of a molecule with an even number of electrons. Details of the structures validating identification of the cyclase substrate, intermediates and product are shown in Supplementary Fig. 3.

support a low level of cyclase activity, with conversion of 16% of the MgPME substrate to $^{13}\text{C}_1$ -hydroxy-MgPME and $^{13}\text{C}_1$ -keto-MgPME intermediates although with no formation of the final product

(Supplementary Fig. 4b). However, the cyclase catalytic cycle was completed, generating the final product DV PChlide *a*, only in the presence of PSI and with light exposure (Extended Data Fig. 2). The

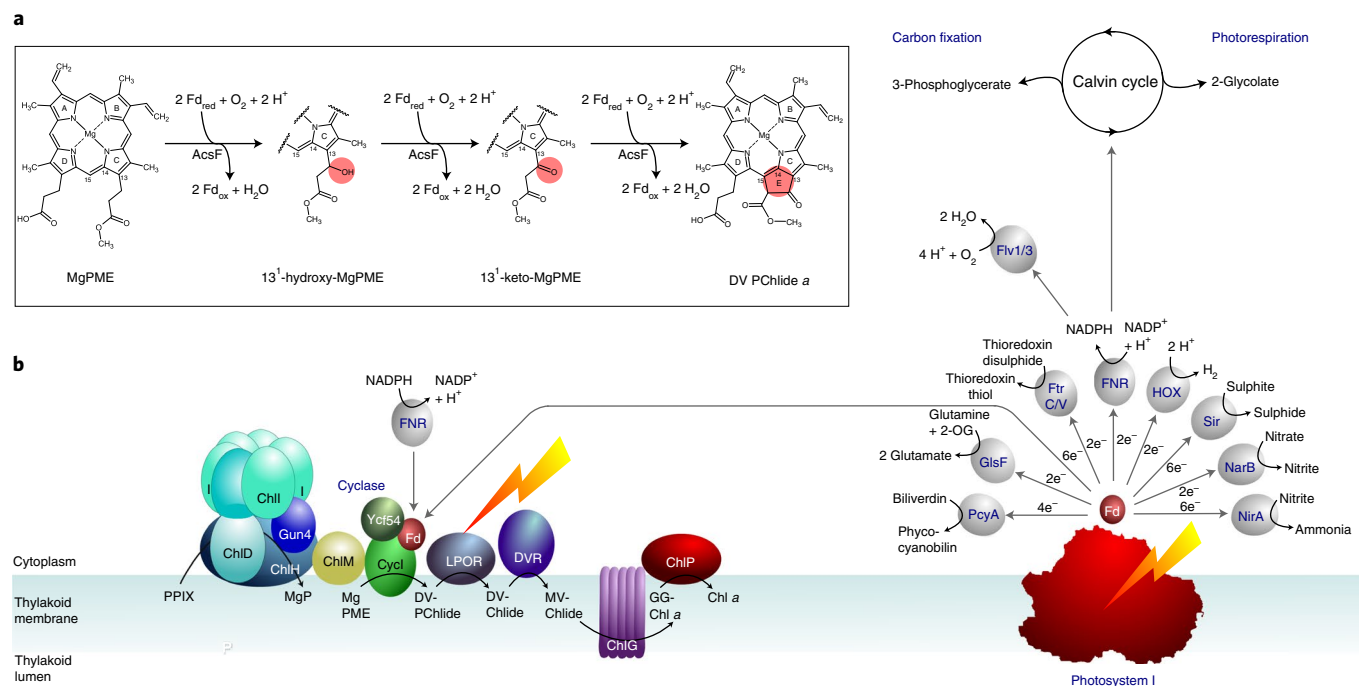


Fig. 6 | Diagram depicting the Fd-dependent cyclase reaction catalysed by AcsF and the supply of reduced Fd, directly or indirectly, by PSI. a, Updated sequence of cyclase reactions catalysed by AcsF, with the chemical change of the porphyrin substrate at each step highlighted by pink circles. Fd_{red} and Fd_{ox} represent reduced and oxidized Fd, respectively. **b**, Left: the chlorophyll biosynthesis pathway is shown, progressing from protoporphyrin IX (PPIX) to chlorophyll *a* (Chl *a*) via magnesium protoporphyrin IX (MgP), Mg-protoporphyrin IX monomethyl ester (MgPME), 3,8-divinyl protochlorophyllide *a* (DV-PChlide), divinyl chlorophyllide *a* (DV-Chlide), monovinyl chlorophyllide *a* (MV-Chlide) and geranylgeranyl-chlorophyll *a* (GG-Chl *a*). ChlH, D and I are subunits, and Gun4 is an accessory protein of the magnesium chelatase complex; ChIM is the MgP methyltransferase; Cycl is the counterpart of the AcsF cyclase in cyanobacteria and plants, shown here with Fd and the accessory protein Ycf54; LPOR is the light-dependent PChlide oxidoreductase; DVR is the divinyl reductase, the cyanobacterial version (BciB) of which requires Fd, whereas plant DVR does not. ChIG is the chlorophyll synthase and ChIP is the geranylgeranyl reductase. Right: depiction of a potential direct link between PSI and chlorophyll biosynthesis, showing that PSI could provide reduced Fd for the cyclase reaction; FNR-based reduction of Fd is also depicted, corresponding to the *in vitro* assays shown in Fig. 3 and Extended Data Fig. 2, respectively. Reduced Fd also provides electrons for a variety of cellular functions, shown here for cyanobacterial metabolism and adapted from the diagram in ref. ⁴¹. PcyA, phycocyanobilin:Fd oxidoreductase; GlsF, Fd-dependent glutamate synthase; FtrC/V, Fd:thioredoxin reductase; FNR, Fd:NADP⁺ reductase; Sir, Fd:sulfite reductase; NarB, nitrate reductase; NirA, nitrite reductase; Flv1/3, Flavodi-iron 1/3; HOX, bidirectional hydrogenase.

production level of DV PChlide *a* was clearly dependent on the PSI level (Extended Data Fig. 2; 1× PSI versus 4× PSI) and was approximately proportional to the duration of light exposure (Extended Data Fig. 2; 15- versus 30-min light). These results clearly show the potential for the cyclase step in chlorophyll biosynthesis to be coupled to the production of reduced Fd and turnover of PSI, a point that will be covered in the Discussion.

Discussion

Over 70 years have elapsed since Granick's proposed reaction sequence for the formation of the isocyclic ring of chlorophyll⁸. The inability to dissect this sequence has represented a large gap in our knowledge of chlorophyll biosynthesis, given that the formation of ring E begins to establish the eventual absorption line-shape of chlorophyll. The presence of ring E, a prerequisite for all chlorophylls and bacteriochlorophylls, extends the π system along the Q_y axis, red shifting and enhancing the Q_y absorption band. The availability of a biochemically pure, O₂-dependent cyclase represented the only prospect of resolving the reaction intermediates, while recent genetic approaches that resolved the enigmatic subunit composition of the O₂-dependent cyclase^{4,21} paved the way for recombinant production of the enzyme for *in vitro* analysis. In the present study, we overexpressed a single-subunit cyclase, *Rvi. gelatinosus* AcsF, in *E. coli* and purified the enzyme to homogeneity. The pale brown colour and iron content of the purified AcsF protein, combined with

the ~340-nm charge transfer band as well as the distinctive absorbance bands when in complex with azide, provide experimental evidence that AcsF is indeed a di-iron protein. Sequence alignments of certain AcsF proteins and their putative di-iron ligands are shown in Extended Data Fig. 3a, while Extended Data Fig. 3b,c shows how the di-iron ligands of AcsF might be coordinated based on motifs shared between AcsF proteins and the soluble methane mono-oxygenase hydroxylase subunit from *Methylococcus capsulatus*.

Because AcsF is a mono-oxygenase, O₂ activation is part of its catalytic cycle, which requires a source of electrons. Our reconstitution tests showed that NADPH may be the ultimate electron source but not the direct electron donor, because an oxidoreductase (FNR) and an electron mediator (Fd) were also required to form the electron transfer chain that supports cyclase activity (Fig. 2e). We were able to reconstitute cyclase activity using either spinach FNR and Fd (Fig. 2) or recombinantly produced *Anabaena* counterparts (Fig. 3) which, taken together with the *in vivo* heterologous activity of AcsF shown in *E. coli*²¹, indicate that the AcsF reaction probably shares a generic electron transfer chain with other metabolic processes. In its native host, *Rvi. gelatinosus*, AcsF relies on the reduced Fd generated by the Rnf system³⁵, which utilizes the proton motive force to derive electrons from NADH to Fd, and/or a flavin-based electron bifurcation system³⁶ that oxidizes NADH to produce reduced Fd and ubiquinol simultaneously. The cyclase from oxygenic photoautotrophs is also expected to use reduced Fd as the electron source,

given that cyanobacterial, green algal and plant cyclases are active in *E. coli*^{21,37}, and cyanobacterial and plant cyclases are functional in *Rvi. gelatinosus*^{43,37}. Intriguingly, a recent report has already connected cyclase activity with plastidal FNR in plants³⁸. Furthermore, while our paper was being reviewed, a report emerged showing that the in vitro activity of the barley cyclase requires Fd³⁹. It is conceivable that the requirement for additional electron transfer partners eluded early cyclase characterizations that used complex cellular fractions. The finding of Fd involvement is notable because it points to a potential connection between cyclase and the photosynthetic electron transport chain, linking chlorophyll biosynthesis to photosynthetic activity and/or the redox state of thylakoid membranes⁴⁰. Despite this potential direct link to PSI, NADPH/FNR/Fd was the most effective source of electrons for assay of cyclase in vitro (Fig. 4) which, if replicated in vivo, would allow the 'dark' synthesis of DV PChlide *a*. This route for Fd reduction is shown in Fig. 6, in addition to a more direct, PSI-coupled source of electrons. The ultimate source of reduced FNR and Fd is PSI, and the O₂-dependent cyclase adds a candidate to the list of metabolic functions supported by PSI⁴¹. As proof of principle, we devised an assay that couples the catalytic cycle of cyclase with the provision of reduced Fd by PSI (Extended Data Fig. 2). Figure 6 depicts this dependence of chlorophyll biosynthesis on PSI turnover, and it shows that the light-dependent stage in chlorophyll biosynthesis, catalysed by light-dependent PChlide oxidoreductase (LPOR), is preceded by a cyclase step that, albeit indirectly, is also light dependent.

The AcsF cyclase displays classic Michaelis–Menten kinetic behaviour regarding the porphyrin substrate, MgPME. The Michaelis–Menten constant, K_M , was determined to be 7.0 μM (Fig. 3d), typical of chlorophyll biosynthetic enzymes such as LPOR and magnesium chelatase from *Synechocystis*, with K_M values of 8.6 μM for PChlide⁴² and 3.2 μM for deuteroporphyrin IX⁴³, respectively. The K_d for MgPME binding to AcsF is 0.16 μM (Fig. 3f,g), somewhat lower than that for magnesium chelatase ($K_d = 1.2 \mu\text{M}$ for deuteroporphyrin IX)³¹ and the methyltransferase ($K_d = 2.4 \mu\text{M}$ for Mg-deuteroporphyrin IX)⁴⁴. The K_M for MgPME greatly exceeds K_d , due to the complexity of the reaction undertaken by AcsF and its reliance on both FNR and Fd during the reaction cycle. This K_M value is also probably influenced by β -DDM detergent molecules associated with AcsF, and with the hydrophobic MgPME substrate, with consequent effects on product release. Thus, the low turnover number, k_{cat} , of 0.9 min^{-1} with respect to MgPME (Fig. 3d) reflects the complexity of the catalytic sequence that consists of multiple sequential reactions, each of which requires two electrons supplied by a coupled redox reaction. The value of k_{cat} is comparable with the 0.8 min^{-1} measured for magnesium chelatase⁴³, both of which are much slower than the 57 s^{-1} obtained for the methyltransferase^{44,45}, which precedes cyclase in the chlorophyll biosynthesis pathway. In regard to NADPH, the kinetic data were best described by the Hill equation and showed positive cooperativity ($n = 2.1$) (Fig. 3e), which arises from the multiple sequential, NADPH-dependent reactions required to form the final product.

The availability of an in vitro cyclase assay enabled us to isolate and identify the progression of chemical species en route to the DV PChlide *a* product. The amounts of purified enzyme and porphyrin substrate could be varied to adjust the levels of cyclase reaction intermediates and final product, and the MS identification method minimized the potential interference from undefined protein components, pigment impurities and artefacts. We conclusively identified 13¹-hydroxy-MgPME and 13¹-keto-MgPME as reaction intermediates on the basis of the m/z of their radical cations and the specific transition of the precursor ion to product ions (Fig. 5 and Supplementary Fig. 3). As the reaction proceeded, these two pigment species showed the transition from initial accumulation to subsequent dissipation (Fig. 4), characteristic of reaction intermediates. The hydrophobicity and spectral features of

13¹-hydroxy-MgPME are consistent with previous studies involving cucumber and *C. reinhardtii* cyclase systems (Fig. 4, peak X1)^{14,46}. 13¹-keto-MgPME was demonstrated to be a cyclase substrate with chemically synthesized pigments¹⁴, but had not been detected directly in any cyclase system to date. The spectroscopic properties of 13¹-keto-MgPME (Fig. 4, peak X2) match those of the synthetic version¹⁴, and position the pigment between MgPME and DV PChlide *a*, reminiscent of the 'longer-wavelength metalloporphyrins' detected in cucumber cotyledons⁴⁷. We did not detect any pigment species suggestive of a 13¹–13² acrylate derivative of MgPME in the assay by HPLC or MS analysis, consistent with a report that the synthetic acrylate derivative is not a cyclase substrate²⁰. The reaction sequence, signposted by the reaction intermediates identified by MS, is depicted in Fig. 6a. We note that although there is no final product, DV PChlide *a*, AcsF can support limited (16%) conversion of MgPME substrate, forming low levels of the 13¹-hydroxy and 13¹-keto intermediates (Supplementary Fig. 4b) and possibly indicating different redox requirements for the three steps of the catalytic cycle. Although the in vitro assay with FNR/Fd could convert all MgPME to DV PChlide *a*, further work is required to investigate electron donors in vivo, and the mechanism by which reduced Fd serves as the direct electron donor to the di-iron centre of AcsF. Mechanistic details of the activation of molecular oxygen within the AcsF cyclase, a di-iron enzyme, require the application of spectroscopic and structural techniques.

In summary, our work removes the last remaining hurdle in the study of the O₂-dependent cyclase by showing that reduced Fd serves as the direct electron donor to the di-iron centre of AcsF. Our approaches for expression, purification and reconstitution of cyclase are transferrable to the study of the other two classes of O₂-dependent cyclase, which require auxiliary Ycf54 or BciE subunits⁴. The unambiguous identification of the two reaction intermediates provides an insight into the catalytic mechanism, which should be further investigated by mutagenesis and structural studies to pinpoint the key residues involved in the formation of the isocyclic ring. In addition, a detailed analysis of the interaction between Fd and AcsF should be performed in future to establish the Fd binding site that promotes electron transfer during the catalytic cycle.

Methods

Production and purification of AcsF, Fd and FNR. The *acsF* gene (RGE_33550) was amplified from the genomic DNA of *Rvi. gelatinosus* using the forward primer 5'-GAGTCTCATATGCTCGCGACCCGACGATCG-3' and the reverse primer 5'-GAGTCTGGATCCTCACCATGCCGGGCCATG-3' and cloned into the NdeI/BamHI sites of the pET14b vector, resulting in the pET14b-AcsF plasmid. Gene fragments encoding *Anabaena* Fd (P0A3C8) and FNR (P21890; lacking the N-terminal 136 amino acids) were synthesized (Integrated DNA Technologies) with codon optimization for expression in *E. coli*, and cloned into the NcoI/HindIII sites of the pET28a vector to create plasmids pET28a-Fd and pET28a-FNR, respectively. The nucleotide sequences of synthesized genes are listed in Supplementary Table 1. The strains *E. coli* C43(DE3), BL21(DE3) and BL21(DE3) ΔiscR ⁴⁸ were used for overexpression of AcsF, FNR and Fd, respectively. *E. coli* strains were grown in TB medium (12 g l^{-1} tryptone, 24 g l^{-1} yeast extract, 10 g l^{-1} glycerol, 2.31 g l^{-1} KH₂PO₄, 12.54 g l^{-1} K₂HPO₄) for AcsF and Fd, and in LB medium for FNR, with 100 $\mu\text{g ml}^{-1}$ ampicillin or 30 $\mu\text{g ml}^{-1}$ kanamycin where required. Cultures were grown at 37°C with shaking at 220 r.p.m. then shifted to either 30°C for AcsF and FNR or 28°C for Fd, with shaking at 175 r.p.m. for induction. For C43(DE3)/pET14b-AcsF, 1/50 of starter culture was inoculated and the culture grown for 5 h before 0.4 mM isopropyl- β -D-thiogalactopyranoside (IPTG) and 0.1 g l^{-1} ferric ammonium citrate were added. After 24-h induction, cells were harvested and resuspended in buffer A (25 mM MOPS-NaOH pH 7.5, 10 mM MgCl₂, 500 mM NaCl, 10% (vol/vol) glycerol, 20 mM imidazole). For BL21(DE3)/pET28a-FNR, a 1/100 inoculum was used and the culture grown to an optical density (OD)₆₀₀ of 0.6–0.8 before induction with 0.25 mM IPTG. Cells were harvested after 20-h induction and resuspended in 20 mM Tris-HCl pH 9.0. A 1/100 inoculum was used for BL21(DE3) ΔiscR /pET28a-Fd, and the culture grown to an OD₆₀₀ of 0.6–0.8 before supplementation with 0.25 mM IPTG and 0.1 g l^{-1} ferric ammonium citrate. After 24-h induction, cells were harvested and resuspended in 20 mM Tris-HCl pH 7.4. All cell suspensions were flash-frozen in liquid N₂ and stored at –20°C.

For purification of AcsF, cells were defrosted and supplemented with DNase I, lysozyme and proteinase inhibitor cocktail (Sigma-Aldrich) before incubation at room temperature with shaking for 20 min. Cells were disrupted by one passage through a French pressure cell at 18,000 pounds per square inch and eight cycles of 30-s sonication, followed by centrifugation at 43,399g at 10°C for 30 min. The resulting pellet was resuspended in buffer A. Then, β -DDM was added at a concentration of 1% (wt/vol) and solubilization performed at 4°C on a tube roller for 1 h. Insoluble material was removed by centrifugation at 43,399g at 10°C for 30 min. The soluble fraction was diluted twofold with buffer A and applied to Ni²⁺-loaded Chelating Sepharose Fast Flow resin (GE Healthcare), washed with buffer B (25 mM MOPS-NaOH pH 7.5, 10 mM MgCl₂, 500 mM NaCl, 10% glycerol, 100 mM imidazole, 0.04% β -DDM) and protein eluted with buffer C (25 mM MOPS-NaOH pH 7.5, 10 mM MgCl₂, 100 mM NaCl, 10% glycerol, 400 mM imidazole, 0.04% β -DDM). Protein-containing fractions were pooled and exchanged into buffer D (50 mM MES-NaOH pH 6.0, 10 mM MgCl₂, 500 mM NaCl, 10% glycerol, 0.04% β -DDM) using a PD-10 column (GE Healthcare). Following the addition of 2 mM ferrous ammonium sulphate, the protein solution was incubated at 4°C on a tube roller for 1 h, clarified by centrifugation at 21,380g at 4°C for 10 min and loaded onto a HiLoad 16/600 Superdex 200 prep-grade gel filtration column (GE Healthcare) equilibrated with buffer D and eluted at 0.4 ml min⁻¹ using an ÄKTAprius plus instrument monitored by PrimeView 5.0 (hereafter used for all gel filtration and ion exchange chromatography). Soluble protein standards from the Gel Filtration Markers Kit for 29–700 kDa (Sigma-Aldrich) and membrane protein standards, kindly provided by D. Swainsbury, University of Sheffield, were analysed using the same gel filtration method. Calibration curves were generated using SigmaPlot 14.0 and used to estimate the molecular mass of AcsF, whose concentration was determined by absorbance at 280 nm using an extinction coefficient of 59,820 M⁻¹ cm⁻¹, calculated by the ProtParam tool in the ExPASy portal⁴⁹.

For purification of FNR, cell breakage was conducted as per the purification of AcsF but passage through a French pressure cell was omitted. The cell lysate was clarified by centrifugation at 43,399g at 10°C for 30 min, passed through a 0.45- μ m filter and applied to a HiTrap QHP anion exchange column (GE Healthcare). The column was washed with 20 mM Tris-HCl pH 9.0, and proteins were eluted with a linear gradient of 0–0.25 M NaCl in 20 mM Tris-HCl pH 9.0 over 200 ml. Fractions containing FNR were pooled and concentrated before loading onto a HiLoad 16/600 Superdex 200 prep-grade gel filtration column (GE Healthcare) equilibrated with buffer E (20 mM HEPES-NaOH pH 7.5, 100 mM NaCl) and eluted at 0.5 ml min⁻¹. For purification of Fd, cell breakage was conducted as for purification of AcsF. The cell lysate was clarified and subjected to anion exchange chromatography as for the purification of FNR, except that a linear gradient of 0–0.5 M NaCl in 20 mM Tris-HCl pH 7.4 over 200 ml was used for elution. Fractions containing Fd were pooled and subjected to ammonium sulphate precipitation three times at 0°C to remove contaminants. Solid ammonium sulphate was added directly to the protein solution until cloudy, and protein contaminants were removed by centrifugation. Fd was recovered from the clarified solution by performing ammonium sulphate precipitation twice with 100% saturated solution at 0°C, reconstituted with ~5 ml 20 mM Tris-HCl pH 7.4 and purified by gel filtration as for FNR. Fd-containing fractions were pooled and subjected twice to ammonium sulphate precipitation with 100% saturated solution at 0°C to remove potential nucleic acid contamination. Recovered Fd was finally dissolved in buffer E. Concentrations of co-factor-containing FNR and Fd were determined by absorbance using reported extinction coefficients of 9,400 M⁻¹ cm⁻¹ at 458 nm for FNR and 7,200 M⁻¹ cm⁻¹ at 423 nm for Fd⁵⁰.

Iron quantification. The iron content of purified AcsF protein was determined using an iron assay kit (Sigma-Aldrich) according to the manufacturer's instructions. Assays were conducted in triplicate and data were analysed using SigmaPlot v.14.0.

Absorbance spectroscopy. Spectra were recorded on either a Cary 60 UV-vis spectrophotometer (Cary WinUV Scan Application v.5.1.0.1016) or an Omega Fluostar microplate reader (BMG LABTECH, Reader Control software v.5.50 R4) equipped with an LVis plate. To record the AcsF–sodium azide spectrum, 16 μ M AcsF was mixed with an equal volume of 4 M sodium azide stock solution prepared in buffer D and the mixture incubated at room temperature for 30 min. The absorbance spectrum was recorded using 2 M sodium azide in buffer D as blank.

Purification of MgPME. MgPME was extracted from a *Rvi. gelatinosus* $\Delta bchE\Delta acsF$ mutant as described previously²¹. The resulting MgPME solution was vacuum dried, reconstituted in a minimal volume of 0.2% (wt/vol) ammonia in methanol and purified on an Agilent 1200 HPLC system (ChemStation for LC 3D systems B.04.02) using a Fortis C₁₈ reverse-phase column (particle size 5 μ m, 150 mm \times 10 mm). Pigments were eluted at 40°C at 2.5 ml min⁻¹ with a linear gradient from 35% (vol/vol) solvent A (350 mM ammonium acetate, 30% (vol/vol) methanol) to 75% (vol/vol) solvent B (methanol) over 35 min and monitored by absorbance at 416 nm. Fractions containing MgPME were collected, mixed with 0.5-vol ultra-pure H₂O (QH₂O) and loaded onto a Discovery DSC-18 SPE tube column (Sigma-Aldrich) for solid-phase extraction. The column was washed with

QH₂O to remove ammonium acetate. MgPME was eluted with methanol, vacuum dried and stored at –20°C. MgPME concentration was estimated by absorbance at 589 nm using an extinction coefficient of 18,000 M⁻¹ cm⁻¹ in methanol¹¹.

Differential scanning calorimetry. Purified AcsF was centrifuged at 16,000g at 4°C for 10 min to remove potential aggregates and diluted to 1 mg ml⁻¹ in buffer D, then 300 μ l of diluted AcsF solution was loaded into a NanoDSC (TA Instruments) and subjected to a heat ramp of 1°C min⁻¹. After removal of the start-up hook, the data were converted to molar heat capacity using NanoAnalyze v.11.0 and exported to Igor Pro 8.04 for processing by a cubic spline baseline fit, followed by a Gaussian fit whose modal value was reported as the melting point.

End-point HPLC-based cyclase assays. Spinach Fd, FNR, bovine catalase and NADPH were obtained from Sigma-Aldrich. Assays were conducted in buffer F (100 mM TES-NaOH, 50 mM HEPES-NaOH pH 7.7, 10 mM MgCl₂, 1 M glycerol, 0.04% β -DDM) with 3.7 μ M AcsF, 0.2 mg ml⁻¹ spinach Fd, 0.4 U ml⁻¹ spinach FNR, 2 mM NADPH, 10 μ M MgPME (added from 200 μ M MgPME stock solution prepared in 0.2% ammonia in methanol) and 0.29 mg ml⁻¹ catalase. To test the co-factor requirement for cyclase activity, AcsF, Fd, FNR and NADPH were omitted where indicated. For reaction intermediate determination, 20 μ M MgPME was used and AcsF was added at incrementally doubled concentrations from 0.23 to 3.68 μ M. Assays were performed in 50- μ l volumes in 1.5-ml Eppendorf tubes and initiated with the addition of AcsF, followed by incubation at 30°C in the dark with shaking at 175 r.p.m. for 30 min. Then, 200 μ l of 0.2% ammonia in methanol was added to stop the assay and 35 μ l of the clarified pigment extract was analysed by HPLC as described previously³⁷. Elution of pigment species was monitored by absorbance at 416 and 440 nm and fluorescence emission at 595 and 640 nm (excitation at 440 nm).

Coupled PSI cyclase assays. Asc and DCPIP were obtained from Sigma-Aldrich. Purified spinach PSI and Pc were kindly provided by G. Mayneord, University of Sheffield. Assays were conducted in buffer F with 2 μ M AcsF, 0.04 mg ml⁻¹ spinach Fd, 14 μ M MgPME, spinach PSI containing 6 or 22.4 μ M Chl *a*, 20 μ M spinach Pc, 2 mM Asc, 60 μ M DCPIP and 0.29 mg ml⁻¹ catalase. AcsF, Fd, PSI, Pc, Asc and DCPIP were omitted where indicated, to test the co-factor dependency of cyclase activity. Assays were performed in 50- μ l volumes in 1.5-ml Eppendorf tubes and incubated at 30°C, either in the dark for 30 min or under illumination from two red, light-emitting diode bicycle tail lights (50 lumens, WQJifv) for 15 or 30 min. Assays were stopped by the addition of 4 vol 0.2% ammonia in methanol, and 20 μ l of the clarified pigment extract was analysed by HPLC as described previously²¹. Pigment elution was monitored by fluorescence emission at 640 nm (excitation at 440 nm).

Continuous absorbance-based cyclase assays. Assays were performed in buffer F with AcsF, *Anabaena* Fd, *Anabaena* FNR, NADPH and MgPME at concentrations specified in the figure legends, and with catalase at 0.29 mg ml⁻¹. Assays were conducted at 30°C in 100- μ l volumes in Greiner μ clear F-bottom medium-binding 96-well black microplates. Assays were initiated by the addition of AcsF, and the reaction progress was monitored using an Omega microplate reader (BMG LABTECH, Reader Control software 5.50 R4) in absorbance mode for 30 min. Spectra from 400 to 750 nm were recorded for each well every 30–60 s (depending on the number of assays). Initial rates (v_i) were calculated using the software supplied by the manufacturer (MARS 3.32 R5). Kinetic parameters were determined by fitting equation (1) to the data with nonlinear regression using Igor Pro 8.04. Errors were determined from least-squares analysis of the fits. DV PChlide *a* concentration was estimated by absorbance at 634 nm using an extinction coefficient of 19,796 M⁻¹ cm⁻¹ (refs. ^{29,30}).

$$v_i = \frac{k_{\text{cat}}[E][S]}{K_M + [S]} \quad (1)$$

$$v_i = \frac{k_{\text{cat}}[E][S]^n}{(K_{0.5})^n + [S]^n} \quad (2)$$

where k_{cat} is the turnover number, [E] is the enzyme concentration, [S] is the substrate concentration, K_M is the Michaelis–Menten constant, n is the Hill coefficient and $K_{0.5}$ is the substrate concentration that gives half-maximal reaction rate in the Hill equation.

Tryptophan fluorescence quenching binding assays. Assays were conducted by mixing 0.2 μ M AcsF in buffer D with an equal volume of MgPME solution prepared in buffer G (0.02% (wt/vol) ammonia, 10% (vol/vol) methanol, 90% (vol/vol) buffer D) at concentrations incrementally doubled from 40 nM to 80 μ M. The mixture was incubated at 30°C for 2 min, and then fluorescence spectra between 300 and 400 nm (10-nm bandpass) were recorded on a FluoroMax 3 fluorimeter (HORIBA Jobin Yvon) (FluorEssence Package 3.9) at 30°C with excitation at 280 nm (5-nm bandpass). A modified, single-site binding equation (equation (3)), which takes into account the inner filter effect of light absorbance by MgPME^{31,32},

was fitted to the obtained titration data with nonlinear regression using Igor Pro v.8.04:

$$F_{\text{obs}} = F_0 + F_{\text{max}} \frac{[L]_{\text{T}} + [E]_{\text{T}} + K_d - \sqrt{([L]_{\text{T}} + [E]_{\text{T}} + K_d)^2 - 4[L]_{\text{T}}[E]_{\text{T}}}}{2[E]_{\text{T}}} + M[L]_{\text{T}} \quad (3)$$

where F_{obs} is observed fluorescence, F_0 is initial fluorescence, F_{max} is the maximum amplitude of fluorescence quenching, $[L]_{\text{T}}$ is total ligand concentration, $[E]_{\text{T}}$ is total enzyme concentration (fixed at 0.1 μM during the fitting procedure), K_d is the apparent dissociation constant and M is the inner filter contribution of ligand.

Pigment analysis by LC-ESI-MS/MS. Scaled-up in vitro assays were conducted as per the end-point HPLC-based cyclase assay with 0.92 μM AcsF. The resulting pigment extract was mixed with 2 vol QH₂O and subjected to solid-phase extraction as per MgPME purification. Pigments were eluted with methanol, followed by vacuum drying and reconstitution in 50 μl of 70% (vol/vol) methanol (LC grade), of which 5 μl was analysed by capillary-flow liquid chromatography (Dionex RSLCnano system, Thermo Scientific) coupled online to a QExactive HF quadrupole-Orbitrap mass spectrometer (Thermo Scientific). Analytes were separated on a Luna C₁₈ reverse-phase column (particle size 5 μm , pore size 100 \AA , 250 mm \times 1 mm; Phenomenex) operating at 50 $\mu\text{l min}^{-1}$ and 40 $^{\circ}\text{C}$, with a linear gradient from 35% (vol/vol) solvent A to 75% (vol/vol) solvent B over 35 min. The mass spectrometer was controlled by Thermo Xcalibur 4.0.27.42 and fitted with a heated electrospray ionization source operating with the following parameters: spray voltage 3,500 V positive, capillary temperature 320 $^{\circ}\text{C}$, sheath gas 35 units. For full-scan profile MS acquisition, the following parameters were used: range 500–700 m/z , resolution 120,000, automatic gain control target 1×10^6 and maximum fill time 200 ms. Product ion scans were performed by centroid parallel reaction monitoring with selection of ions at 598.24, 614.24, 612.22 and 611.21 m/z for MgPME, 13¹-hydroxy-MgPME, 13¹-keto-MgPME and DV PChlide *a*, respectively, and at an isolation width of 1.2 m/z . Other parameters were set thus: resolution 30,000, automatic gain control target 2×10^5 , maximum fill time 100 ms and stepped collision energy 30/35/40 eV. Mass spectra were extracted from the output data files and compared with theoretical relative isotopomer ion intensity values using Xcalibur 4.0.27.42. Mapping of precursor and product ion masses to their structures was carried out with the aid of ACD/ChemSketch 2019.1.3. These structures were then exported to Xara Xtreme v.5.1.1.9166 to produce the figures.

Reporting Summary. Further information on research design is available in the Nature Research Reporting Summary linked to this article.

Data availability

All supporting data are included in the Supplementary Information. The mass spectrometry raw data files used for Fig. 5 and Supplementary Fig. 3 have been deposited to <https://figshare.shef.ac.uk/articles/dataset/13655774>. Source data are provided with this paper.

Received: 2 September 2020; Accepted: 8 February 2021;
Published online: 15 March 2021

References

- Porra, R. J. et al. Origin of the two carbonyl oxygens of bacteriochlorophyll *a*. Demonstration of two different pathways for the formation of ring E in *Rhodobacter sphaeroides* and *Roseobacter denitrificans*, and a common hydratase mechanism for 3-acetyl group formation. *Eur. J. Biochem.* **239**, 85–92 (1996).
- Porra, R. J., Urzinger, M., Winkler, J., Bubenzer, C. & Scheer, H. Biosynthesis of the 3-acetyl and 13¹-oxo groups of bacteriochlorophyll *a* in the facultative aerobic bacterium, *Rhodovulum sulfidophilum*: the presence of both oxygenase and hydratase pathways for isocyclic ring formation. *Eur. J. Biochem.* **257**, 185–191 (1998).
- Wiesselmann, M. et al. Mg-protoporphyrin IX monomethyl ester cyclase from *Rhodobacter capsulatus*: radical SAM-dependent synthesis of the isocyclic ring of bacteriochlorophylls. *Biochem. J.* **477**, 4635–4654 (2020).
- Chen, G. E., Canniffe, D. P. & Hunter, C. N. Three classes of oxygen-dependent cyclase involved in chlorophyll and bacteriochlorophyll biosynthesis. *Proc. Natl Acad. Sci. USA* **114**, 6280–6285 (2017).
- Pinta, V., Picaud, M., Reiss-Husson, F. & Astier, C. *Rubrivivax gelatinosus acsF* (previously *orf358*) codes for a conserved, putative binuclear-iron-cluster-containing protein involved in aerobic oxidative cyclization of Mg-protoporphyrin IX monomethylester. *J. Bacteriol.* **184**, 746–753 (2002).
- Hollingshead, S. et al. Conserved chloroplast open-reading frame *ycf54* is required for activity of the magnesium protoporphyrin monomethylester oxidative cyclase in *Synechocystis* PCC 6803. *J. Biol. Chem.* **287**, 27823–27833 (2012).
- Albus, C. A. et al. LCAA, a novel factor required for magnesium protoporphyrin monomethylester cyclase accumulation and feedback control of aminolevulinic acid biosynthesis in tobacco. *Plant Physiol.* **160**, 1923–1939 (2012).
- Granick, S. The structural and functional relationships between heme and chlorophyll. *Harvey Lect. Ser.* **44**, 220–245 (1950).
- Chereskin, B. M. & Castelfranco, P. A. Effects of iron and oxygen on chlorophyll biosynthesis: II. Observations on the biosynthetic pathway in isolated etiochloroplasts. *Plant Physiol.* **69**, 112–116 (1982).
- Chereskin, B. M., Wong, Y. S. & Castelfranco, P. A. In vitro synthesis of the chlorophyll isocyclic ring: transformation of magnesium-protoporphyrin IX and magnesium-protoporphyrin IX monomethyl ester into magnesium-2,4-divinyl pheoporphyrin *a*₃. *Plant Physiol.* **70**, 987–993 (1982).
- Nasrullah-Boyce, A., Griffiths, W. T. & Jones, O. T. The use of continuous assays to characterize the oxidative cyclase that synthesizes the chlorophyll isocyclic ring. *Biochem. J.* **243**, 23–29 (1987).
- Walker, C. J., Mansfield, K. E., Smith, K. M. & Castelfranco, P. A. Incorporation of atmospheric oxygen into the carbonyl functionality of the protochlorophyllide isocyclic ring. *Biochem. J.* **257**, 599–602 (1989).
- Wong, Y. S. & Castelfranco, P. A. Resolution and reconstitution of Mg-protoporphyrin IX monomethyl ester (oxidative) cyclase, the enzyme system responsible for the formation of the chlorophyll isocyclic ring. *Plant Physiol.* **75**, 658–661 (1984).
- Bollivar, D. W. & Beale, S. I. Formation of the isocyclic ring of chlorophyll by isolated *Chlamydomonas reinhardtii* chloroplasts. *Photosynth. Res.* **43**, 113–124 (1995).
- Bollivar, D. W. & Beale, S. I. The chlorophyll biosynthetic enzyme Mg-protoporphyrin IX monomethyl ester (oxidative) cyclase: characterization and partial purification from *Chlamydomonas reinhardtii* and *Synechocystis* sp. PCC 6803. *Plant Physiol.* **112**, 105–114 (1996).
- Rzeznicka, K. et al. *Xantha-1* encodes a membrane subunit of the aerobic Mg-protoporphyrin IX monomethyl ester cyclase involved in chlorophyll biosynthesis. *Proc. Natl Acad. Sci. USA* **102**, 5886–5891 (2005).
- Ellsworth, R. K. & Aronoff, S. Investigations on the biogenesis of chlorophyll *a*: III. Biosynthesis of Mg-vinylpheoporphine *a*₃ methylester from Mg-protoporphyrin IX monomethylester as observed in *Chlorella* mutants. *Arch. Biochem. Biophys.* **125**, 269–277 (1968).
- Ellsworth, R. K. & Aronoff, S. Investigations of the biogenesis of chlorophyll *a*: IV. Isolation and partial characterization of some biosynthetic intermediates between Mg-protoporphyrin IX monomethyl ester and Mg-vinylpheoporphine *a*₃, obtained from *Chlorella* mutants. *Arch. Biochem. Biophys.* **130**, 374–383 (1969).
- Wong, Y. S. & Castelfranco, P. A. Properties of the Mg-protoporphyrin IX monomethyl ester (oxidative) cyclase system. *Plant Physiol.* **79**, 730–733 (1985).
- Walker, C. J. et al. The magnesium-protoporphyrin IX (oxidative) cyclase system: studies on the mechanism and specificity of the reaction sequence. *Biochem. J.* **255**, 685–692 (1988).
- Chen, G. E. et al. Complete enzyme set for chlorophyll biosynthesis in *Escherichia coli*. *Sci. Adv.* **4**, eaaq1407 (2018).
- Miroux, B. & Walker, J. E. Over-production of proteins in *Escherichia coli*: mutant hosts that allow synthesis of some membrane proteins and globular proteins at high levels. *J. Mol. Biol.* **260**, 289–298 (1996).
- Strop, P. & Brunger, A. T. Refractive index-based determination of detergent concentration and its application to the study of membrane proteins. *Protein Sci.* **14**, 2207–2211 (2005).
- Fox, B. G., Shanklin, J., Somerville, C. & Münck, E. Stearoyl-acyl carrier protein Δ^9 desaturase from *Ricinus communis* is a diiron-oxo protein. *Proc. Natl Acad. Sci. USA* **90**, 2486–2490 (1993).
- Makris, T. M., Chakrabarti, M., Münck, E. & Lipscomb, J. D. A family of diiron monooxygenases catalyzing amino acid beta-hydroxylation in antibiotic biosynthesis. *Proc. Natl Acad. Sci. USA* **107**, 15391–15396 (2010).
- Behan, R. K. & Lippard, S. J. The aging-associated enzyme CLK-1 is a member of the carboxylate-bridged diiron family of proteins. *Biochemistry* **49**, 9679–9681 (2010).
- Shanklin, J. & Somerville, C. Stearoyl-acyl-carrier-protein desaturase from higher plants is structurally unrelated to the animal and fungal homologs. *Proc. Natl Acad. Sci. USA* **88**, 2510–2514 (1991).
- Choi, Y. S., Zhang, H., Brunzelle, J. S., Nair, S. K. & Zhao, H. In vitro reconstitution and crystal structure of *p*-aminobenzoate *N*-oxygenase (AurF) involved in aureothin biosynthesis. *Proc. Natl Acad. Sci. USA* **105**, 6858–6863 (2008).
- Helfrich, M., Ross, A., King, G. C., Turner, A. G. & Larkum, A. W. D. Identification of [8-vinyl]-protochlorophyllide *a* in phototrophic prokaryotes and algae: chemical and spectroscopic properties. *Biochim. Biophys. Acta* **1410**, 262–272 (1999).
- Klement, H., Helfrich, M., Oster, U., Schoch, S. & Rüdiger, W. Pigment-free NADPH:protochlorophyllide oxidoreductase from *Avena sativa* L: purification and substrate specificity. *Eur. J. Biochem.* **265**, 862–874 (1999).

31. Karger, G. A., Reid, J. D. & Hunter, C. N. Characterization of the binding of deuteroporphyrin IX to the magnesium chelatase H subunit and spectroscopic properties of the complex. *Biochemistry* **40**, 9291–9299 (2001).
32. Meneely, K. M., Sundlov, J. A., Gulick, A. M., Moran, G. R. & Lamb, A. L. An open and shut case: the interaction of magnesium with MST enzymes. *J. Am. Chem. Soc.* **138**, 9277–9293 (2016).
33. Schäfer, M., Drayß, M., Springer, A., Zacharias, P. & Meerholz, K. Radical cations in electrospray mass spectrometry: formation of open-shell species, examination of the fragmentation behaviour in ESI-MSⁿ and reaction mechanism studies by detection of transient radical cations. *Eur. J. Org. Chem.* **2007**, 5162–5174 (2007).
34. Jensen, K., Johnston, J. B., de Montellano, P. R. O. & Møller, B. L. Photosystem I from plants as a bacterial cytochrome P450 surrogate electron donor: terminal hydroxylation of branched hydrocarbon chains. *Biotechnol. Lett.* **34**, 239–245 (2012).
35. Biegel, E., Schmidt, S., González, J. M. & Müller, V. Biochemistry, evolution and physiological function of the Rnf complex, a novel ion-motive electron transport complex in prokaryotes. *Cell. Mol. Life Sci.* **68**, 613–634 (2011).
36. Buckel, W. & Thauer, R. K. Energy conservation via electron bifurcating ferredoxin reduction and proton/Na⁺ translocating ferredoxin oxidation. *Biochim. Biophys. Acta* **1827**, 94–113 (2013).
37. Chen, G. E. & Hunter, C. N. Protochlorophyllide synthesis by recombinant cyclases from eukaryotic oxygenic phototrophs and the dependence on Ycf54. *Biochem. J.* **477**, 2313–2325 (2020).
38. Herbst, J., Girke, A., Hajirezaei, M. R., Hanke, G. & Grimm, B. Potential roles of YCF54 and ferredoxin-NADPH reductase for magnesium protoporphyrin monomethylester cyclase. *Plant J.* **94**, 485–496 (2018).
39. Stuart, D. et al. Aerobic barley Mg-protoporphyrin IX monomethyl ester cyclase is powered by electrons from ferredoxin. *Plants* **9**, 1157 (2020).
40. Steccanella, V., Hansson, M. & Jensen, P. E. Linking chlorophyll biosynthesis to a dynamic plastoquinone pool. *Plant Physiol. Biochem.* **97**, 207–216 (2015).
41. Lea-Smith, D. J., Bombelli, P., Vasudevan, R. & Howe, C. J. Photosynthetic, respiratory and extracellular electron transport pathways in cyanobacteria. *Biochim. Biophys. Acta* **1857**, 247–255 (2016).
42. Heyes, D. J., Martin, G. E., Reid, R. J., Hunter, C. N. & Wilks, H. M. NADPH:protochlorophyllide oxidoreductase from *Synechocystis*: overexpression, purification and preliminary characterisation. *FEBS Lett.* **483**, 47–51 (2000).
43. Reid, J. D. & Hunter, C. N. Magnesium-dependent ATPase activity and cooperativity of magnesium chelatase from *Synechocystis* sp. PCC6803. *J. Biol. Chem.* **279**, 26893–26899 (2004).
44. Shepherd, M. & Hunter, C. N. Transient kinetics of the reaction catalysed by magnesium protoporphyrin IX methyltransferase. *Biochem. J.* **382**, 1009–1013 (2004).
45. Shepherd, M., Reid, J. D. & Hunter, C. N. Purification and kinetic characterization of the magnesium protoporphyrin IX methyltransferase from *Synechocystis* PCC6803. *Biochem. J.* **371**, 351–360 (2003).
46. Wong, Y. S., Castelfranco, P. A., Goff, D. A. & Smith, K. M. Intermediates in the formation of the chlorophyll isocyclic ring. *Plant Physiol.* **79**, 725–729 (1985).
47. Rebeiz, C. A., Mattheis, J. R., Smith, B. B., Rebeiz, C. C. & Dayton, D. F. Chloroplast biogenesis: biosynthesis and accumulation of Mg-protoporphyrin IX monoester and longer wavelength metalloporphyrins by greening cotyledons. *Arch. Biochem. Biophys.* **166**, 446–465 (1975).
48. Walters, K. A. & Golbeck, J. H. Designing a modified clostridial [2[4Fe–4S] ferredoxin as a redox coupler to directly link photosystem I with a Pt nanoparticle. *Photosynth. Res.* **143**, 165–181 (2020).
49. Artimo, P. et al. ExPASy: SIB bioinformatics resource portal. *Nucleic Acids Res.* **40**, W597–W603 (2012).
50. Pueyo, J. J. & Gómez-Moreno, C. Purification of ferredoxin-NADP⁺ reductase, flavodoxin and ferredoxin from a single batch of the cyanobacterium *Anabaena* PCC 7119. *Prep. Biochem.* **21**, 191–204 (1991).
51. Whittington, D. A. & Lippard, S. J. Crystal structures of the soluble methane monooxygenase hydroxylase from *Methylococcus capsulatus* (Bath) demonstrating geometrical variability at the dinuclear iron active site. *J. Am. Chem. Soc.* **123**, 827–838 (2001).

Acknowledgements

We thank D. Swainsbury, University of Sheffield, for providing membrane protein standards for gel filtration calibration and N. Soulier, The Pennsylvania State University, for supplying the BL21(DE3) Δ iscR strain. G.E.C., N.B.P.A. P.J.J. and C.N.H. thank the Biotechnology and Biological Sciences Research Council (BBSRC UK, award no. BB/M000265/1) for financial support. C.N.H. is also supported by European Research Council Synergy Award no. 854126. M.J.D. was supported by BBSRC UK (award no. BB/M012166/1).

Author contributions

G.E.C., N.B.P.A., P.J.J., M.J.D. and C.N.H. designed the research. G.E.C., N.B.P.A. and P.J.J. performed research and analysed data. G.E.C., N.B.P.A., P.J.J., M.J.D. and C.N.H. wrote the manuscript.

Competing interests

The authors declare no competing interests.

Additional information

Extended data is available for this paper at <https://doi.org/10.1038/s41477-021-00876-3>.

Supplementary information The online version contains supplementary material available at <https://doi.org/10.1038/s41477-021-00876-3>.

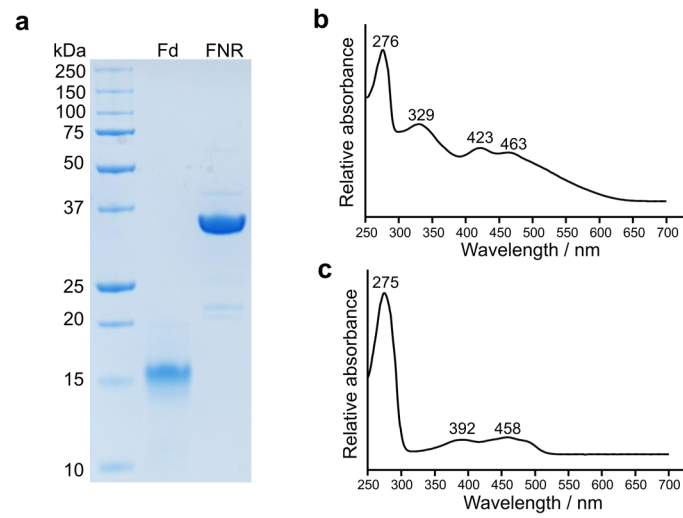
Correspondence and requests for materials should be addressed to G.E.C. or C.N.H.

Peer review information *Nature Plants* thanks Bernhard Grimm and the other, anonymous, reviewer(s) for their contribution to the peer review of this work.

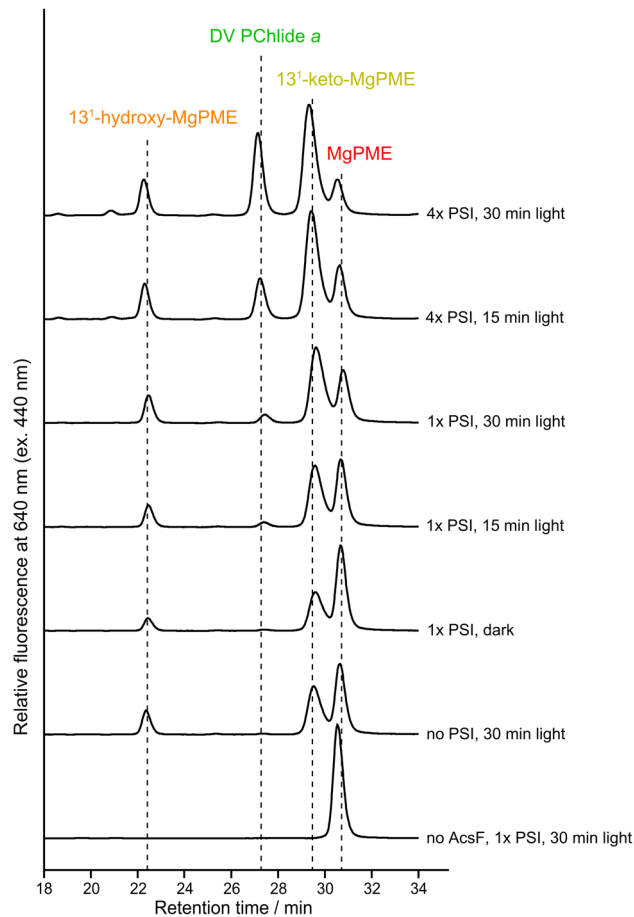
Reprints and permissions information is available at www.nature.com/reprints.

Publisher's note Springer Nature remains neutral with regard to jurisdictional claims in published maps and institutional affiliations.

© The Author(s), under exclusive licence to Springer Nature Limited 2021



Extended Data Fig. 1 | Analysis of purified *Anabaena* Fd and FNR. a, SDS-PAGE analysis of purified *Anabaena* Fd and FNR. **b,** Absorbance spectrum of purified *Anabaena* Fd. **c,** Absorbance spectrum of purified *Anabaena* FNR.



Extended Data Fig. 2 | HPLC elution profiles of pigment extracts from coupled PSI-cyclase assays. A complete assay contained $2 \mu\text{M}$ AcsF, 0.04 mg ml^{-1} spinach Fd, $14 \mu\text{M}$ MgPME, spinach PSI containing 6 (1x PSI) or $22.4 \mu\text{M}$ (~ 4 x PSI) Chl *a*, $20 \mu\text{M}$ spinach Pc, 2 mM Asc, $60 \mu\text{M}$ DCPIP and 0.29 mg ml^{-1} catalase. Assays were incubated either in the dark for 30 min, or under red light illumination for 15 or 30 min. Pigment extracts from the assays were analysed by HPLC and pigment elution was monitored by fluorescence at 640 nm excited at 440 nm. Pigment species were identified by retention times and fluorescence spectra (as in Fig. 4). See Supplementary Fig. 4a for HPLC analysis of pigment extracts from additional control assays.

a

```

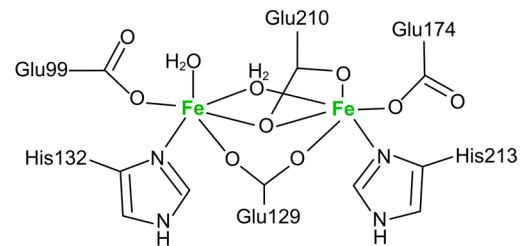
CycI      98  EFSGFLLYKELGRRLKKNPLLAECFNLMsRDEARHAGFLNKAMSDFNLSLDLGLFLTKSRKYTFFKPKFIYATYLSEKIGYWRYYITTYRHLKKNPNDCIYPIFEFFENWCQDENRH 214
CHL27    143 EFSGFLLYKELGRRLKKTNPVVAEIFSLMSRDEARHAGFLNKGLSDFNALDLGLFLTKARKYTFFKPKFIYATYLSEKIGYWRYYITTYRHLKENPEFQCYPIFKYFENWCQDENRH 259
CRD1     141 EFSGFLLYKELARRMKASSPEVAEMFLMSRDEARHAGFLNKALSDFNALDLGLFLTKNRITYTFKPKFIYATYLSEKIGYWRYYITTYRHLQRNPDNQFYPLFEYFENWCQDENRH 257
CTH1     141 EFSGFLLYKELGRRLKATNPVVAEIFTLMSRDEARHAGFLNKAMSDFNALDLGLFLTKNRKYTFFKPKFIYATYLSEKIGYWRYYITTYRHLQRNPDNQLYPLFEYFENWCQDENRH 257
AcsF     99  EFSGCVLYNEIQKNV--ENPDVKALMRYMARDESRHAGFINQALRDFGLGIDLGLKRTKAYTFKPKFIYATYLSEKIGYARYITTYRQLERHPDKRFHPFRWFERWCNDEFRH 213
0294    103 EFSGCVLYKEMKRRG--SNPDIRELFNYMARDEARHAGFINDALREAGVAVNLGFLTKAKKYTYFRPKFIYATYLSEKIGYARYITTYRHLLEANPEHRFHPIFKWFKWCNDEFRH 217
          **** :*:*: :. : * : : *:*:*:*:*:*:*:*:*:* :. : : : : : * * : : *:*:*:* *:*:*:*:* *:*:*:*:* : : : : : : : : : : * *

```

b

CycI	E -X ₃₁ - E AR H -X ₄₁ - E -X ₃₅ - E NR H
CHL27	E -X ₃₁ - E AR H -X ₄₁ - E -X ₃₅ - E NR H
CRD1	E -X ₃₁ - E AR H -X ₄₁ - E -X ₃₅ - E NR H
CTH1	E -X ₃₁ - E AR H -X ₄₁ - E -X ₃₅ - E NR H
AcsF	E -X ₂₉ - E SR H -X ₄₁ - E -X ₃₅ - E FR H
0294	E -X ₂₉ - E AR H -X ₄₁ - E -X ₃₅ - E FR H
MMOH	E -X ₂₉ - E IR H -X ₆₁ - E -X ₃₃ - E LR H

c



Extended Data Fig. 3 | The diiron binding motif and proposed diiron ligation of AcsF. **a**, Sequence alignments showing the conserved diiron binding motif of AcsF proteins. Sequences are from *Synechocystis* sp. PCC 6803 (CycI, BAA16583), *Arabidopsis thaliana* (CHL27, NP_191253), *Chlamydomonas reinhardtii* (CRD1, XP_001692557; CTH1, XP_001691047), *Rubrivivax gelatinosus* IL144 (AcsF, BAL96694) and *Rhodobacter sphaeroides* 2.4.1 (0294, abbreviated for RSP_0294, YP_353369). Conserved, highly similar and similar residues are marked with asterisks, colons and full stops, respectively. The putative diiron ligands are in red and bold. Full-length protein sequences were used for alignments but for clarity, only the putative diiron binding motifs with the residue range indicated, are shown. **b**, Sequence homologies between the diiron binding motifs of AcsF proteins and the soluble methane monooxygenase hydroxylase subunit from *Methylococcus capsulatus* Bath (MMOH, P22869). **c**, Proposed coordination of the diiron ligands of AcsF at the diferrous state based on the crystal structure of MMOH (PDB, 1FYZ)⁵¹.

Reporting Summary

Nature Research wishes to improve the reproducibility of the work that we publish. This form provides structure for consistency and transparency in reporting. For further information on Nature Research policies, see our [Editorial Policies](#) and the [Editorial Policy Checklist](#).

Statistics

For all statistical analyses, confirm that the following items are present in the figure legend, table legend, main text, or Methods section.

n/a Confirmed

- The exact sample size (n) for each experimental group/condition, given as a discrete number and unit of measurement
- A statement on whether measurements were taken from distinct samples or whether the same sample was measured repeatedly
- The statistical test(s) used AND whether they are one- or two-sided
Only common tests should be described solely by name; describe more complex techniques in the Methods section.
- A description of all covariates tested
- A description of any assumptions or corrections, such as tests of normality and adjustment for multiple comparisons
- A full description of the statistical parameters including central tendency (e.g. means) or other basic estimates (e.g. regression coefficient) AND variation (e.g. standard deviation) or associated estimates of uncertainty (e.g. confidence intervals)
- For null hypothesis testing, the test statistic (e.g. F , t , r) with confidence intervals, effect sizes, degrees of freedom and P value noted
Give P values as exact values whenever suitable.
- For Bayesian analysis, information on the choice of priors and Markov chain Monte Carlo settings
- For hierarchical and complex designs, identification of the appropriate level for tests and full reporting of outcomes
- Estimates of effect sizes (e.g. Cohen's d , Pearson's r), indicating how they were calculated

Our web collection on [statistics for biologists](#) contains articles on many of the points above.

Software and code

Policy information about [availability of computer code](#)

Data collection

Gel filtration: PrimeView 5.0 (GE Healthcare) to control the ÄKTAprime plus instrument and acquire data.
Absorption spectra: BMG LABTECH Reader Control software 5.50 R4 to control the the Omega FluoStar microplate reader equipped with an LVis plate and acquire data, Cary WinUV Scan Application 5.1.0.1016 to control the Cary 60 UV-vis spectrophotometer and acquire data.
High performance liquid chromatography (HPLC): ChemStation for LC 3D systems B.04.02 to control the Agilent 1200 HPLC system and acquire data.
Steady-state kinetics: BMG LABTECH Reader Control software 5.50 R4 to control the the Omega FluoStar microplate reader and acquire data
Tryptophan fluorescence quenching assay: FluorEssence Package 3.9, a modified version of Origin, to control the Jobin Yvon HORIBA Fluoromax 3 fluorometer and acquire data.
Mass spectrometry: Thermo Xcalibur 4.0.27.42 to control the Q Exactive HF instrument and acquire data.
Differential scanning calorimetry analysis: NanoAnalyze 3.11.0 to control the NanoDSC (TA Instruments) and acquire data.

Data analysis

Data was exported in either .csv or .xls format using the softwares listed in 'Data collection'. The exported data were used to prepare graphs using SigmaPlot 14.0 or OriginPro 2019b 9.6.5.169 or Igor Pro 8.04. Graphs were exported to Xara Xtreme 5.1.1.9166 to produce figures.
For gel filtration and iron assay data analysis, nonlinear regression analysis and curve fit were performed using SigmaPlot 14.0.
Extinction coefficients of proteins were calculated using the ProtParam tool in the ExPASy portal (<https://web.expasy.org/protparam/>).
For steady-state kinetic data analysis, initial rates of product formation were calculated in the BMG LABTECH MARS Data Analysis software 3.32 R5 by quantifying the product absorbance at 634 nm using a reported extinction coefficient, and exported in .csv format.
For steady-state kinetic and tryptophan fluorescence quenching data analysis, nonlinear regression analysis and curve fit were performed using Igor Pro 8.04.
For differential scanning calorimetry data analysis, curve fit was performed using Igor Pro 8.04.
Mass spectra were extracted from the output data-files and compared with theoretical relative isotopomer ion intensity values using Xcalibur

4.0.27.42 (Thermo Scientific). Mapping precursor and product ion masses to their structures was carried out with the aid of ACD/ChemSketch 2019.1.3. These structures were exported to Xara Xtreme 5.1.1.9166 to produce figures.

For manuscripts utilizing custom algorithms or software that are central to the research but not yet described in published literature, software must be made available to editors and reviewers. We strongly encourage code deposition in a community repository (e.g. GitHub). See the Nature Research [guidelines for submitting code & software](#) for further information.

Data

Policy information about [availability of data](#)

All manuscripts must include a [data availability statement](#). This statement should provide the following information, where applicable:

- Accession codes, unique identifiers, or web links for publicly available datasets
- A list of figures that have associated raw data
- A description of any restrictions on data availability

All supporting data are included in the Supplementary Information. Annotated source data are provided with this paper for Figs. 2b, 2c, 2e, 4, Extended Data Figs. 1, 2, and Supplementary Figs. 1, 4a, 4b. The mass spectrometry raw data-files used for Fig. 5 and Supplementary Fig. 3 have been deposited to <https://figshare.shef.ac.uk/articles/dataset/13655774>.

Field-specific reporting

Please select the one below that is the best fit for your research. If you are not sure, read the appropriate sections before making your selection.

- Life sciences Behavioural & social sciences Ecological, evolutionary & environmental sciences

For a reference copy of the document with all sections, see nature.com/documents/nr-reporting-summary-flat.pdf

Life sciences study design

All studies must disclose on these points even when the disclosure is negative.

Sample size	The sample size was not predetermined by statistical method. For steady-state kinetic study, tryptophan fluorescence quenching assay and iron assay, experiments were conducted in triplicate (n=3). This number of repeats is standard within biochemical and enzymological studies. The data sets for kinetic and biophysical experiments show there is clearly sufficient signal to noise to be able to robustly analyse the results. Mass spectrometry data were derived from two samples taken from a single preparation. The sample volume was fixed by the injection loop volume on the chromatography system and the sample concentration was sufficient to allow analysis of the spectra without saturating the ion detection system, thereby maintaining optimal mass accuracy. The first sample was analysed by full-MS acquisition and the second sample by parallel reaction monitoring.
Data exclusions	No data were excluded.
Replication	For absorption spectra, gel filtration analysis, end-point HPLC-based enzymatic assays, experiments were repeated 2-3 times, giving very similar results. For steady-state kinetic study, tryptophan fluorescence quenching assay and iron assay, experiments were conducted in triplicate and signals from triplicates were comparable. The reproducibility of steady-state enzymatic assays were also confirmed by including appropriate positive (saturating substrate conditions) and negative (no substrate conditions) controls. For mass spectrometry, the chromatography and spectral acquisition methods were optimised with 2 full-MS analyses on a test sample batch. For the final sample batch, 3 full-MS and 2 parallel reaction monitoring analyses were performed. In all cases, spectral interpretation was successful and identical within each acquisition method.
Randomization	Randomization was not performed. This study involved the analysis of specific enzymes and pigments. As such, randomization would be inappropriate, making rationalization of the results impossible.
Blinding	Blinding was not possible because the samples were prepared and the data obtained by the same investigators.

Reporting for specific materials, systems and methods

We require information from authors about some types of materials, experimental systems and methods used in many studies. Here, indicate whether each material, system or method listed is relevant to your study. If you are not sure if a list item applies to your research, read the appropriate section before selecting a response.

Materials & experimental systems

n/a	Included in the study
<input checked="" type="checkbox"/>	<input type="checkbox"/> Antibodies
<input checked="" type="checkbox"/>	<input type="checkbox"/> Eukaryotic cell lines
<input checked="" type="checkbox"/>	<input type="checkbox"/> Palaeontology and archaeology
<input checked="" type="checkbox"/>	<input type="checkbox"/> Animals and other organisms
<input checked="" type="checkbox"/>	<input type="checkbox"/> Human research participants
<input checked="" type="checkbox"/>	<input type="checkbox"/> Clinical data
<input checked="" type="checkbox"/>	<input type="checkbox"/> Dual use research of concern

Methods

n/a	Included in the study
<input checked="" type="checkbox"/>	<input type="checkbox"/> ChIP-seq
<input checked="" type="checkbox"/>	<input type="checkbox"/> Flow cytometry
<input checked="" type="checkbox"/>	<input type="checkbox"/> MRI-based neuroimaging